

Adaptive least-squares RTM with applications to subsalt imaging

Chong Zeng¹, Shuqian Dong¹, and Bin Wang¹

Abstract

Least-squares reverse time migration (LSRTM) refines the seismic image toward true reflectivity by inversion. Its iterative nature and modeling capability enable the use of synthetic data to guide the preconditioning of input data. When the velocity contains errors, dynamic warping can be used to shift the input data and force the traveltimes to be consistent with the imperfect migration velocity. A crosscorrelation-based confidence level is introduced to control the quality of dynamic warping for field data. The confidence level also is used as an inverse weighting to adaptively precondition the data residual. The adaptive preconditioning automatically balances data fitting in the shallow and deep and speeds up convergence in subsalt. Both synthetic and field data experiments based in the Gulf of Mexico show that the adaptive LSRTM can improve the image quality in subsalt effectively and efficiently. Within only a few iterations, the adaptive LSRTM suppresses the salt halo artifacts and increases the signal-to-noise ratio in poorly illuminated areas. It also improves the termination of sediments against salt boundaries and enhances subsalt image coherency. Compared with conventional RTM, the adaptive LSRTM image is more favorable to geologic interpretation.

Introduction

Salt basins play an important role in worldwide hydrocarbon exploration. As one of the most important parts of seismic data processing, prestack depth migration produces directly interpretable seismic images critical to guiding further drilling analysis. In practice, imaging subsalt structures has never been an easy task due to the geologic complexity related to salt tectonics. The salt body itself acts as a strong reflecting and refracting lens to scatter most energy emitted from the surface seismic source, thus introducing poor illumination and weak signal-to-noise ratio (S/N) in subsalt areas.

The difficulties in building an accurate subsalt velocity model make subsalt imaging even more challenging. While the model-building technique has been advanced to provide high-resolution velocity models for migration, image quality in areas near and below salt bodies is still unsatisfactory in many cases because of the limitations of the imaging algorithms themselves.

Recently, inversion-based imaging algorithms (Schuster, 1993; Nemeth et al., 1999; Duquet et al., 2000), such as least-squares reverse time migration (LSRTM), have gained the attention of geophysicists (e.g., Tang, 2009; Wong et al., 2011; Dai et al., 2013). Different from conventional migration algorithms based on crosscorrelation imaging condition, LSRTM uses geophysical inversion to iteratively refine the seismic image toward true reflectivity (Dong et al., 2012) and overcome many shortcomings of conventional migration methods.

Previous studies, including field data tests (e.g., Zeng et al., 2014a; Zhang et al., 2015), show that LSRTM can reduce migration artifacts, balance image amplitudes, reveal weak signals, and improve image coherency. These advantages make LSRTM very attractive

for subsalt imaging. However, we must address many practical issues (Wang et al., 2013) to bring LSRTM from the laboratory to production. One major problem is that the original theory of LSRTM requires perfect migration velocity; otherwise, the least-squares data fitting between input and modeled data will be erroneous. Unfortunately, velocity errors always exist in the real world, and it seems unattainable to make the short-wavelength velocity components accurate enough near the salt (Etgen et al., 2014). The data mismatch yields extra artifacts in the data residual and then contaminates the image updating. In particular, large errors can occur at far offsets and late arrivals corresponding to subsalt reflections and cause convergence problems in subsalt areas.

Subsalt images also often suffer from strong salt-related migration artifacts. A typical artifact known as a salt “halo” is a type of noise that parallels the salt flank or base of salt (BOS) and strongly degrades the image near the salt. Because of the strong amplitudes of the halo artifacts and the slow convergence of subsalt inversion, LSRTM typically needs tens of iterations to clarify images near the salt, even when the subsalt velocities are accurate enough. The massive computation cost makes LSRTM almost prohibitive for large 3D projects focusing on subsalt.

Here, we tackle the two major problems of imperfect velocity and strong halo artifacts to promote the applicability of LSRTM for subsalt imaging. We propose an adaptive solution for LSRTM so that it can tolerate minor velocity errors and converge fast in subsalt by automatic suppression of the halo artifacts. We also introduce a quality-control tool named “confidence level” to evaluate least-squares data fitting and adaptively precondition the data residual to speed up the subsalt convergence. The philosophy of this adaptive LSRTM (in short, ALSRTM) method is to enhance the quality of subsalt images using the best available, but imperfect, velocity model with minimum computation cost.

Adaptive data fitting with dynamic warping

To date, all least-squares migration methods are implemented as a type of single parameter inversion that searches only for the solution of seismic reflectivity (or impedance). During the entire inversion procedure, seismic velocity is fed to the program as an input parameter and remains unchanged. Thus, the quality of the LSRTM image relies highly on the velocity-model accuracy. Any error in the velocity will propagate into the inversion and will be amplified during the iterations. In theory, LSRTM requires perfect migration velocity to ensure the convergence. However, in real-world subsalt imaging, it seems that velocity errors are unavoidable. This introduces unwanted time shifts in synthetic waveforms with respect to the input data. Because the synthetic data are modeled using the stacked image as the reflectivity, the zero-offset data and model are always self-consistent. As the offset increases, velocity errors are accumulated gradually during prestack modeling. Thus, the time shift is nonlinear and usually increases with offset.

¹TGS-NOPEC Geophysical Company.

<http://dx.doi.org/10.1190/tle35030253.1>

Figure 1 shows an example of the synthetic seismic wiggles overlaid with corresponding time shifts caused by velocity changes in both the near- and far-offset range. It is clear that the far-offset data are more prone to velocity errors than that in the near-offset range. It also indicates LSRTM may have the convergence problem in subsalt due to the importance of far-offset data for subsalt imaging.

Previously, we used a matching filter to correct the synthetic data so that the waveforms can be aligned to generate reasonable residual waveforms (Zeng et al., 2014b). However, this correction will be canceled when we reverse time migrate the residual, and the gradient is blurred due to using inaccurate velocities for adjoint propagation. To make LSRTM tolerable to minor velocity errors, Luo and Hale (2014) proposed to use dynamic warping (Hale, 2013) to modify the arrival time of the input data and force them to be aligned with the synthetic data. For LSRTM, this data-domain adjustment is feasible because it is done only once before the first iteration and imposes no extra computation cost for the inversion. Since the modeling and migration kernels share the same velocity model, the synthetic data are self-consistent with the migrated image in terms of time-to-depth mapping. After adjusting the input data using synthetic as reference, we can obtain a better-focused image by correctly mapping the time-domain data to the depth-domain image. This concept of using synthetic data as a reference to guide the input data preconditioning is an important feature of the ALSRTM.

Using dynamic warping to adaptively adjust the match between input and synthetic data is not only mathematically efficient, but also physically meaningful. If we consider that the real input data come from a physical earth-modeling process based on true earth reflectivity and true velocity, the warped input data are equivalent to the results from the same modeling based on true earth reflectivity and the derived migration velocity. The true earth reflectivity is the inversion objective of LSRTM, and the true earth velocity is unknown. By directly fitting the raw input and synthetic data, the inversion contains two unknowns (true reflectivity and true velocity) but searches for only one of them. This introduces a stability problem for the inversion. On the contrary, fitting the warped input and synthetic data eliminates the involvement of the true earth velocity and leaves the true earth reflectivity as the only unknown for the solution, thus stabilizing the inversion.

Figure 2 demonstrates the effectiveness of dynamic warping during LSRTM with the presence of velocity errors. We first generate a set of synthetic shot gathers using a perfect velocity and true reflectivity, then migrate them using a velocity model containing errors. The designed velocity errors vary nonlinearly from 1% in the shallow to 6% below the salt. Without dynamic warping (Figure 2a), LSRTM generates extra migration artifacts in the shallow and is unable to correctly image the subsalt. By comparison, the result with dynamic warping applied during the inversion (Figure 2b) presents more coherent events in the shallow and continuous sediment images in the subsalt area. The overall

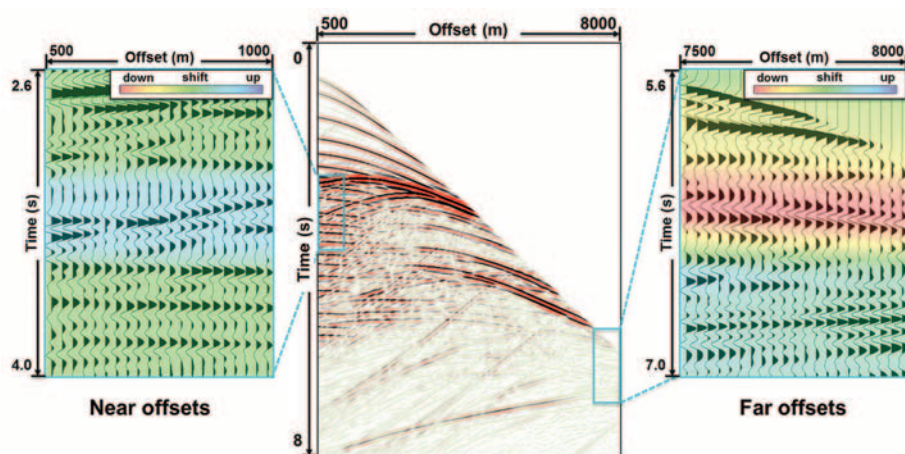


Figure 1. A synthetic example of data shifting caused by velocity errors. The far-offset data are more sensitive to velocity changes than the near-offset data.

image is consistent with the LSRTM result that assumes a perfect velocity model (Figure 2c).

Quality control and adaptive residual preconditioning

When dealing with field data, we should be aware that dynamic warping itself assumes that the differences of the two input signals are minor and mainly due to (temporal or spatial) distortion. Thus, we need to assume that the seismic events in the synthetic data can always be found to match those in the reference data. This assumption is not always true in real-world LSRTM due to the quality limitation of the initial image. Especially for images near the salt, e.g. in the shadow zone or just below the BOS, the image quality is usually poor compared to those above the salt. In addition, extra artifacts on the initial image also will generate spurious events on the synthetic record and therefore degrade the coherency of the synthetic and input waveforms. To overcome this problem, we introduce a confidence level to measure the reliability of the warped data and evaluate the quality of the data adaptive correction. The confidence level at each sample point is calculated by a 2D normalized crosscorrelation using a sliding window in the offset-time domain.

The purpose of the confidence level is to govern the least-squares data fitting for LSRTM. First, it evaluates the initial quality of the input and synthetic data. A high confidence level means the input and synthetic wiggles match well in the scale of dominant period, while a low confidence level suggests adaptive data adjusting should be applied on the input data. A negative confidence-level value indicates a possible cycle skipping because of the change of wiggle polarity after modeling. Moreover, the confidence level tells if the dynamic warping is functional as desired. By comparing the confidence level before and after dynamic warping, we should see an increase of confidence level because the warping algorithm is designed to better align the input and synthetic data.

Figure 3 and Figure 4 demonstrate the procedure of the quality-controlled adaptive data fitting. A real shot gather (Figure 3a) is extracted from a wide-azimuth (WAZ) survey in the Gulf of Mexico (GoM). The corresponding synthetic data (Figure 3b) during the first iteration of LSRTM is presented for comparison. Figure 4a displays the calculated confidence level before the

adaptive data adjusting. The data confidence level is high in the shallow and near-offset range while relatively low in the deep portion and far-offset range. It suggests the velocity contains errors in the deep portion of the model. After applying dynamic warping to the input data and appropriate amplitude correction to the synthetic data, the recalculated confidence level (Figure 4b) increases in the deep portion and far-offset range. The overall confidence level is also increased for the whole gather. It confirms that the dynamic warping appropriately aligns the traveltime of the input and synthetic data by compensating the velocity errors.

The confidence level is also used as an inverse weighting to precondition the data residual to gain optimum convergence focusing on subsalt enhancements. When applying LSRTM to subsalt imaging, we often find that the program needs many iterations to produce notable improvements in the subsalt areas. In the meantime, images above the salt could be overupdated with some undesired artifacts. This is primarily because of the different convergence rates between shallow and deep areas. In most cases, the S/N of the shallow reflections on a shot gather is higher than that in the deep because of the limited illumination and energy penetration below the salt. The corresponding image quality in the shallow is also better than that of subsalt. This means the starting model for the inversion is closer to the true solution in shallow than in deep. Thus, the inversion converges fast in shallow and slowly in deep.

Within the same number of iterations when the subsalt areas yield good waveform fitting between the synthetic and input data, the shallow portion of the synthetic data is likely to overmatch the input containing noise. By preconditioning the raw residual using the confidence level as an inverse weighting, the convergence rates for the shallow and deep images are balanced.

Another important benefit of this adaptive preconditioning is that it automatically dims the strong events on the gradient, including the halos near the BOS or salt flanks, and boosts the weak energy below the salt. This is because the migration operator is linear and directly links the strong events on the depth-domain image with the time-domain data with good S/N and high confidence level. The adaptive weighting guides the inversion to emphasize the weak signals with low confidence level during the iteration until they are recovered to a high confidence level after iterative image updating. In practice, we found this adaptive preconditioning of data residual can speed up the convergence in

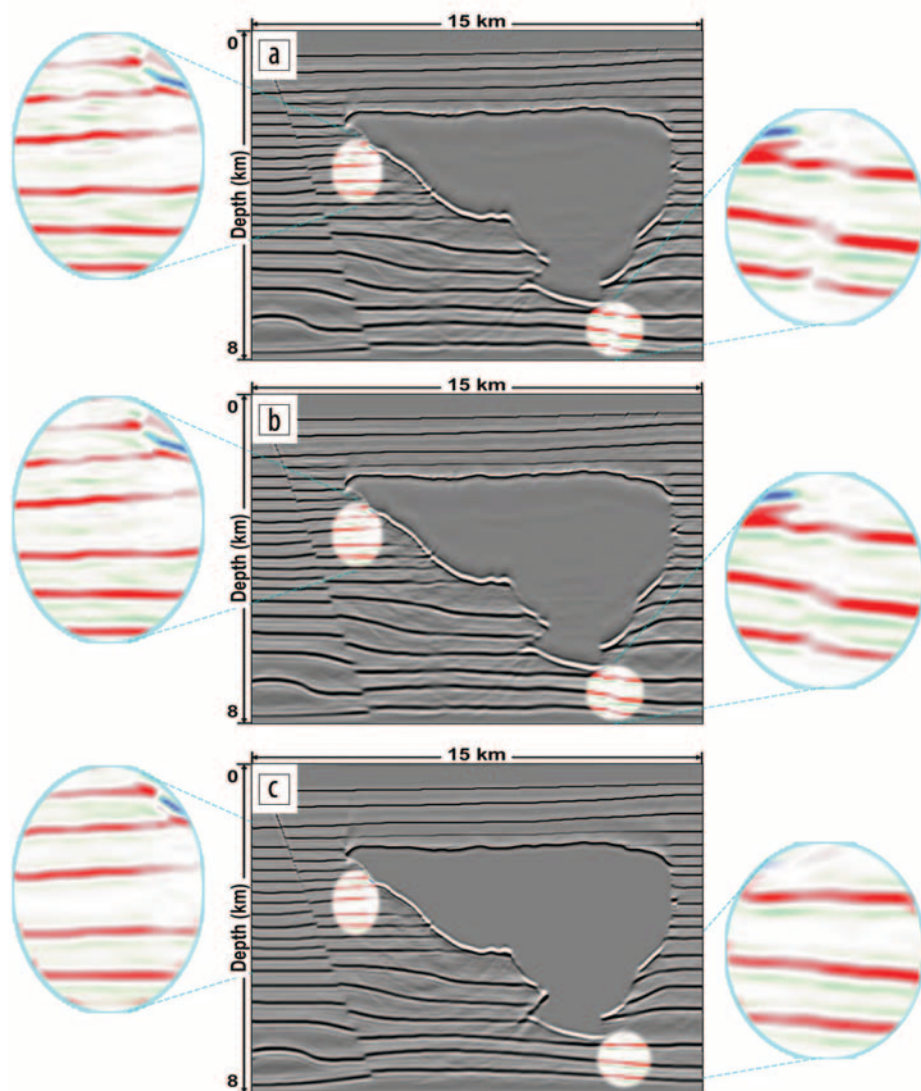


Figure 2. A comparison of synthetic LSRTM results using erroneous migration velocity (a) without and (b) with applying dynamic warping to the input data. The overall image is consistent with (c) the LSRTM result that assumes a perfect velocity model.

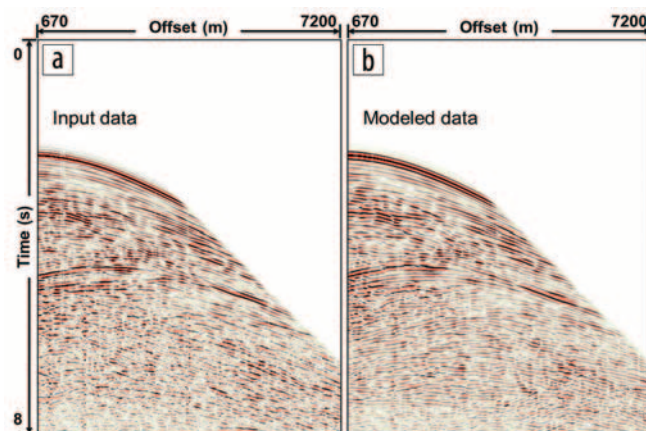


Figure 3. (a) A real shot gather extracted from a survey based in GoM versus (b) the synthetic data during the first iteration of LSRTM.

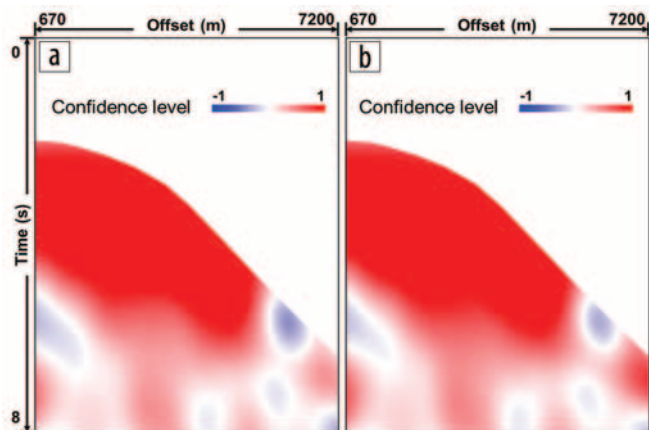


Figure 4. The corresponding confidence level (a) before and (b) after adaptive data adjusting. The confidence level is increased for deep and far-offset reflections after the adaptive data adjusting.

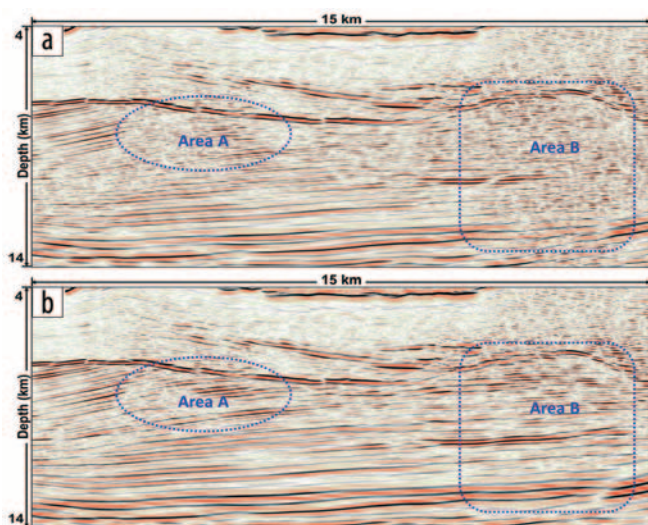


Figure 5. Inline section of (a) conventional RTM image and (b) ALSRTM image migrated from the Freedom 3D WAZ data in the GoM. Area of interest A is marked by the dotted ellipse on the left side. Area of interest B is marked by the rounded rectangle on the right side.

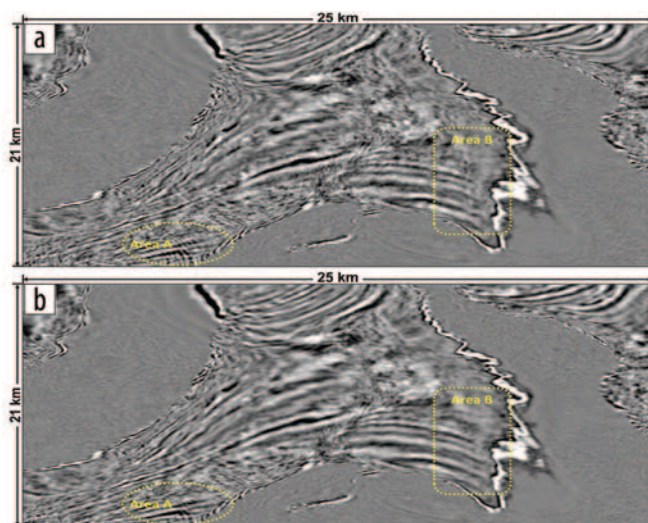


Figure 6. Depth slice of (a) conventional RTM image and (b) ALSRTM image at a depth of 5600 m migrated from the Patriot 3D WAZ data in the GoM. Area A (dotted ellipse) and area B (rounded rectangle) are marked for comparison.

subsalt areas significantly and suppress the strong halo artifacts efficiently so that satisfactory subsalt images can be obtained within only a few iterations.

GoM field data applications

To this point we have developed the ALSRTM focusing on subsalt enhancements. With the quality-controlled adaptive solution, we apply the ALSRTM to the Freedom 3D WAZ data to examine the effectiveness of the algorithm. The survey is a typical WAZ acquisition towing 8-km-long multicable streamers near the Mississippi Canyon in the GoM. Figure 5a shows a target inline section of the conventional RTM image. In area of interest A, which is beneath the BOS, it is very difficult for the interpreters to trace the horizons and determine the location of event termination because of the existence of strong halo artifacts parallel to the salt body. This introduces uncertainties to recover the geologic history of the sedimentation for further analysis.

The image quality in the area of interest B is limited because of a typical illumination problem caused by the salt canopy. The broken image of the BOS also indicates there are potential velocity errors around the salt body. Figure 5b shows the corresponding ALSRTM image using the exact same input data after two iterations. In the area of interest A, the ALSRTM image shows clear geologic contacts between the sediments and the salt body by suppressing the strong halo artifacts. In the area of interest B, the subsalt sediments are better imaged compared to those on the conventional RTM image. The continuity of the subsalt events also is improved because of the increased S/N. The overall comparison suggests that the ALSRTM image offers significant subsalt enhancements and produces favorable interpretation results.

The success of the ALSRTM for subsalt imaging can be confirmed by the application to Patriot 3D WAZ data, which is also from the GoM but in a different survey area. The geologic condition in the Patriot area is more complex than that in the Freedom area. Figure 6a presents a depth slice of the conventional RTM image at a depth of 5600 m. The two salt bodies surround the sediments and cause typical image problems due to the complexity of the wavefield near the steeply dipping salt flanks. Strong migration swings are observed near the salt body in the area marked A.

In area B, the RTM image contains strong halo artifacts that are parallel to the salt boundary and potentially could mislead the interpretation. After the ALSRTM iteration (Figure 6b), the migration swings are reduced and the strong halo artifacts are suppressed to show clear geologic contacts near the salt body.

More detailed image improvements after the ALSRTM are illustrated in a typical inline section shown in Figure 7. The middle part of the conventional RTM section (Figure 7a) contains significant migration swings. In the shadow area near the salt flank, strong low-frequency halo artifacts occur along the overturned salt boundary and bury effective signals from the sediments. By applying the ALSRTM, the middle part of the image (Figure 7b) is more coherent due to the cancellation of the swing noise. The shadow area presents sharp termination of the sediments against the salt boundary after effective suppression of the halo artifacts. It is evident that the quality of the subsalt image after ALSRTM has been enhanced substantially, and the image itself is more geologically interpretable than the conventional RTM image.

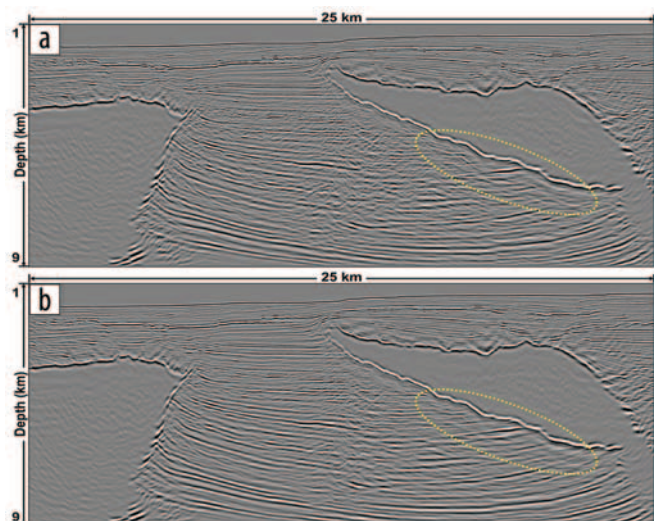


Figure 7. Inline section of the (a) conventional RTM image and (b) ALSRTM image migrated from the Patriot 3D WAZ data. The shadow area is marked by the dotted ellipse.

Conclusions

We addressed typical subsalt imaging problems using LSRTM with quality-controlled adaptive strategies. Minor velocity errors can be compensated by dynamic warping the input data to match the synthetic so that they are consistent with the migration velocity model in both near- and far-offset ranges. The crosscorrelation-based confidence level is developed to qualitatively measure the similarity between the preprocessed input and synthetic data. It also serves as an adaptive weighting to precondition the data residual and automatically balance the data maturity of shallow and deep reflections to gain optimum convergence with emphasis on subsalt enhancements.

The GoM-based field data examples showed that the ALSRTM can improve the quality of subsalt images significantly with relatively low computation cost. Compared to conventional RTM, the ALSRTM suppressed the commonly seen salt-related migration swing noise and halo artifacts to sharpen the termination of sediments against the salt boundaries. It increased the S/N in poorly illuminated areas and enhanced the image coherency of subsalt events. Those subsalt enhancements facilitate the subsequent interpretation and drilling decision. In addition, the adaptive strategies dramatically reduce the computation cost so that the ALSRTM can produce geologically favorable results within only a few iterations. As an overview of the algorithm, the ALSRTM is an effective and efficient imaging technique that is practical to reveal geologic structures near and beneath salt bodies where conventional imaging algorithms encounter challenges. ■■■

Acknowledgments

The authors highly appreciate Jean Ji for the data preparation, Zhigang Zhang for the GPU programming, and Connie Van-Schuyver for the manuscript proofreading. They are grateful to Zhaohong Wu, Darrell Armentrout, Li Li, and Taejong Kim for

their great efforts on field data testing. They also thank Gary Rodriguez, Henrik Roende, and Zhiming Li for continuous support as well as TGS management for permission to publish. The GoM field data are courtesy of TGS and WesternGeco LLC.

Corresponding author: Chong.Zeng@tgs.com

References

- Dai, W., Y. Huang, and G. T. Schuster, 2013, Least-squares reverse time migration of marine data with frequency-selection encoding: *Geophysics*, **78**, no. 4, S233–S242, <http://dx.doi.org/10.1190/geo2013-0003.1>.
- Dong, S., J. Cai, M. Guo, S. Suh, Z. Zhang, B. Wang, and Z. Li, 2012, Least-squares reverse time migration: towards true amplitude imaging and improving the resolution: 82nd Annual International Meeting, SEG, Expanded Abstracts, <http://dx.doi.org/10.1190/segam2012-1488.1>.
- Duquet, B., K. J. Marfurt, and J. A. Dellinger, 2000, Kirchhoff modeling, inversion for reflectivity, and subsurface illumination: *Geophysics*, **65**, no. 4, 1195–1209, <http://dx.doi.org/10.1190/1.1444812>.
- Etgen, J. T., I. Ahmed, and M. Zhou, 2014, Seismic adaptive optics: 84th Annual International Meeting, SEG, Expanded Abstracts, 4411–4415, <http://dx.doi.org/10.1190/segam2014-0867.1>.
- Hale, D., 2013, Dynamic warping of seismic images: *Geophysics*, **78**, no. 2, S105–S115, <http://dx.doi.org/10.1190/geo2012-0327.1>.
- Luo, S., and D. Hale, 2014, Least-squares migration in the presence of velocity errors: *Geophysics*, **79**, no. 4, S153–S161, <http://dx.doi.org/10.1190/geo2013-0374.1>.
- Nemeth, T., C. Wu, and G. T. Schuster, 1999, Least-squares migration of incomplete reflection data: *Geophysics*, **64**, no. 1, 208–221, <http://dx.doi.org/10.1190/1.1444517>.
- Schuster, G. T., 1993, Least-squares cross-well migration: 63rd Annual International Meeting, SEG, Expanded Abstracts, 110–113, <http://dx.doi.org/10.1190/1.1822308>.
- Tang, Y., 2009, Target-oriented wave-equation least-squares migration/inversion with phase-encoded Hessian: *Geophysics*, **74**, no. 6, WCA95–WCA107, <http://dx.doi.org/10.1190/1.3204768>.
- Wang, B., S. Dong, and S. Suh, 2013, Practical aspects of least-squares reverse time migration: 75th Conference and Exhibition, EAGE, Extended Abstracts, <http://dx.doi.org/10.3997/2214-4609.20131000>.
- Wong, M., S. Ronen, and B. Biondi, 2011, Least-squares reverse-time migration/inversion for ocean bottom data: A case study: 81st Annual International Meeting, SEG, Expanded Abstracts, 2369–2373, <http://dx.doi.org/10.1190/1.3627684>.
- Zeng, C., S. Dong, and B. Wang, 2014a, Least-squares reverse time migration: inversion-based imaging toward true reflectivity: *The Leading Edge*, **33**, no. 9, 962–968, <http://dx.doi.org/10.1190/tle33090962.1>.
- Zeng, C., S. Dong, J. Mao, and B. Wang, 2014b, Broadband least-squares reverse time migration for complex structure imaging: 84th Annual International Meeting, SEG, Expanded Abstracts, 3715–3719, <http://dx.doi.org/10.1190/segam2014-1283.1>.
- Zhang, Y., L. Duan, and Y. Xie, 2015, A stable and practical implementation of least-squares reverse time migration: *Geophysics*, **80**, no. 1, V23–V31, <http://dx.doi.org/10.1190/geo2013-0461.1>.